JOURNAL OF APPLIED PHYSICS **119**, 203108 (2016)

Design of coated standing nanowire array solar cell performing beyond the planar efficiency limits

Yang Zeng, Qinghao Ye, and Wenzhong Shen[a]

Institute of Solar Energy, and Key Laboratory of Artificial Structures and Quantum Control (Ministry of Education), Department of Physics and Astronomy, Shanghai Jiao Tong University, Shanghai 200240, People's Republic of China

(Received 6 March 2016; accepted 16 May 2016; published online 31 May 2016)

The single standing nanowire (SNW) solar cells have been proven to perform beyond the planar efficiency limits in both open-circuit voltage and internal quantum efficiency due to the built-in concentration and the shifting of the absorption front. However, the expandability of these nano-scale units to a macro-scale photovoltaic device remains unsolved. The main difficulty lies in the simultaneous preservation of an effective built-in concentration in each unit cell and a broadband high absorption capability of their array. Here, we have provided a detailed theoretical guideline for realizing a macro-scale solar cell that performs furthest beyond the planar limits. The key lies in a complementary design between the light-trapping of the single SNWs and that of the photonic crystal slab formed by the array. By tuning the hybrid HE modes of the SNWs through the thickness of a coaxial dielectric coating, the optimized coated SNW array can sustain an absorption rate over 97.5% for a period as large as 425 nm, which, together with the inherited carrier extraction advantage, leads to a cell efficiency increment of 30% over the planar limit. This work has demonstrated the viability of a large-size solar cell that performs beyond the planar limits. *Published by AIP Publishing.*
[http://dx.doi.org/10.1063/1.4952753]

I. INTRODUCTION

Recent progress on standing nanowire (SNW) solar cells has just revealed the thrilling potential of fabricating a photovoltaic device that performs beyond the Shockley-Queisser (S-Q) limit of conventional solar cells.[1–6] Such possibility is enabled by the unique optical behaviors of the SNWs and was first observed and proposed in the works of Krogstrup *et al.*[1] and Wallentin *et al.*[2] In Krogstrup's work,[1] a single GaAs SNW was found to have an optical cross-section more than 10 times larger than its geometrical cross-section due to the optical antenna effect. They proposed that such built-in concentration of light in a nano-scale device may lead to an increase in open-circuit voltage (V_{oc}) by allowing the electron-hole gas to be generated with a higher chemical potential μ than does the planar S-Q limit.[1,7,8] Although such increment was not experimentally demonstrated due to non-ideal electrical characteristics, it has enlightened the design of a macro-scale solar cell using these nano-scale units to go beyond the traditional limits of solar energy conversion. In Wallentin's work,[2] the viability of this idea was supported by their observation on the InP SNW array solar cell, where they found that the highest V_{oc} exceeded that of the planar cell record despite a large surface area enhancement. Nevertheless, in that work, the cell structure was not purposefully designed to maximize this effect and the overall conversion efficiency is still far from the planar limit. To assess the potential of the single SNW unit cell, our group has previously studied its optical properties and found a direct link between the magnitude of the built-in concentration and the excitation of the $HE_{11\delta}$ and $HE_{12\delta}$ dielectric resonator antenna (DRA) modes.[3] Theoretically, an optimized single SNW cell can possess a conversion efficiency over 33% higher than the planar limit due to the promotion in V_{oc} and the internal quantum efficiency (IQE), showing great promise as a building block for beyond-limit macro-scale photovoltaics.

At present, however, there is still a lack of knowledge of the assembly principles for such a macro-scale device, nor is it clear to what extent can the superior properties of the single SNW unit cells be transferred to their arrays. The difficulty lies in the fact that most previous researches on SNW arrays have either used them as phase-matching antireflection layers[4,9–11] or tuned their resonant absorption by controlling the radius of the SNWs,[2,5,12–19] including the work by Wallentin *et al*. Neither of these two can directly serve our purposes since the radius and array period must be strictly restricted in order to preserve the ability of each unit cell to perform beyond the planar limits.[1,3] Besides, high absorption rate on a macro-scale area must be simultaneously achieved. A more recent work by Nowzari *et al.*[20] on InP nanowire (NW) array solar cell has found that the array pitch plays a crucial role in determining the overall absorption of the SNW array and proposed that the spacing between NWs should be chosen according to the NW diameter. Nevertheless, more detailed discussion on this matter was not provided. Thus, further studies and new methods are needed to fully extend the single SNW solar cell concept into a large-size practical device that performs beyond the traditional boundaries.

In this work, we provide a theoretical guideline for constructing a macro-scale SNW array solar cell that performs

---

[a] Email: wzshen@sjtu.edu.cn. Telephone: +86-21-54747552.

0021-8979/2016/119(20)/203108/9/$30.00 Published by AIP Publishing.

furthest beyond the planar efficiency limits. The two key factors are the tuning of the HE resonant modes by controlling the thickness of a coaxial dielectric coating and the complementary design between the cavity-like light-trapping of single SNWs and the photonic light-trapping of the array. While the former is a premise for preserving the built-in concentration,[1,3] the latter allows it to be fully utilized by sustaining a broadband high absorption capability up to large array periods. By this method, a coated SNW (CSNW) array solar cell with 30% efficiency enhancement over the planar limit has been demonstrated, thus opening up new possibilities for high-efficiency solar cells with novel structures.

II. METHODS

We have performed the simulations based on the typical p-i-n amorphous silicon (a-Si) solar cell structure. All cells, including the planar cell, the SNW cell, and the CSNW cell, have the same configuration from top down: 80 nm transparent conductive oxide (TCO), 20 nm p-a-Si, 460 nm i-a-Si, 20 nm n-a-Si, and metal back reflector (a schematic is drawn for the SNW cell in Fig. 1(a)).[21,22] The radii of the SNW cell and the CSNW cell (the a-Si core) are kept constant at 50 nm, and the coating thickness of the CSNW cell is varied between 0 and 200 nm.

We have employed the finite-difference time-domain (FDTD) method to obtain the optical absorption of the cells. An infinite plane wave is projected vertically onto the cells, which is normal incidence for the planar cell and axial incidence for the SNW and CSNW cells. The incident wavelength λ ranges from 300 nm to 720 nm, covering the major absorption spectrum of a-Si ($E_g = 1.72$ eV). The simulation region is 200 nm × 200 nm × 1 μm with periodic in-plane boundaries for the planar cell, 4 μm × 4 μm × 1 μm with perfectly matched layer in-plane boundaries for the single SNW and single CSNW cells, and $P \times P \times 1$ μm with periodic in-plane boundaries for the SNW array and CSNW array cells, where P is the array period. A mesh refinement of down to 1 nm is applied and the complex refractive indexes n, k of the materials are taken from a widely used reference.[23] The upper limit of the planar cell performance is defined as that under the total-absorption condition, which is obtained by artificially dividing the simulated planar absorption rate $Abs(\lambda)$ by a factor of $[1 - R(\lambda)]$ prior to subsequent electrical simulations, where $R(\lambda)$ is the simulated reflectance from the planar cell.

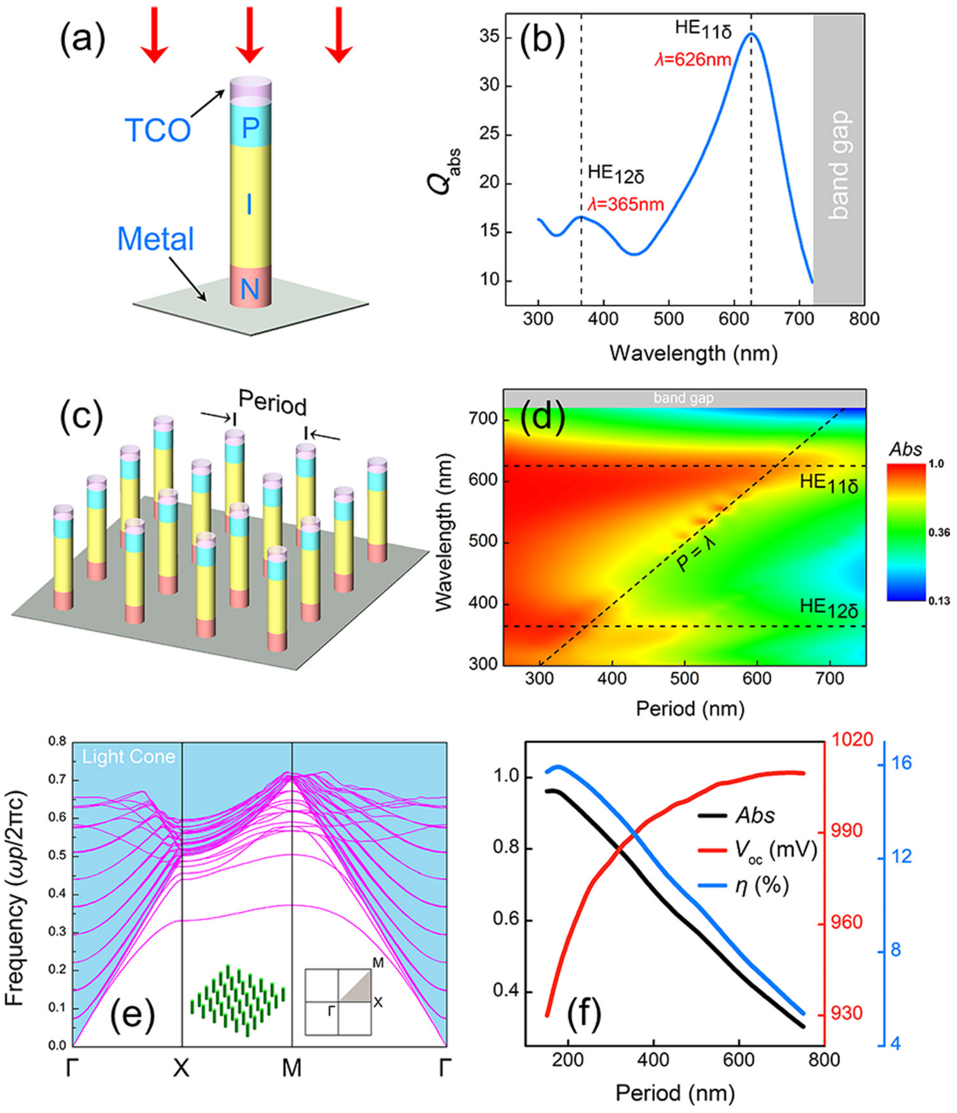

FIG. 1. (a) and (b) Schematic 3D drawing of the single SNW solar cell and its absorption efficiency Q_{abs} as a function of wavelength. The cell radius is 50 nm. (c) and (d) Schematic 3D drawing of the SNW array solar cell and its wavelength-dependent absorption Abs as a function of array period P. Resonant wavelengths of the $HE_{11\delta}$ and $HE_{12\delta}$ modes of the single SNW cell are shown as horizontal dashed lines. (e) Photonic band structure of the SNW array with a period of $P = 300$ nm. The purple lines show the first 40 bands between the labeled high-symmetry points. The blue shaded area is the line cone defined by $\omega = ck$. (f) Simulated AM1.5-integrated absorption Abs, open-circuit voltage V_{oc}, and cell efficiency η of the SNW array solar cell as functions of the array period P.

The electrical simulations of the cells are performed by solving basic semiconductor equations on a tetragonal mesh with a fine mesh size of 1 nm. The photocarrier generation rate at each mesh point is calculated by integrating $Abs(\lambda)$ with the AM1.5 solar spectrum in the interval of 300 nm–720 nm. The TCO and metal contacts are assumed to be ohmic and the semiconductor band gap of a-Si is set as 1.72 eV. Both the Shockley-Read-Hall recombination and Auger recombination are taken into account, giving electron diffusion lengths of ~500 nm in the i-a-Si layer and ~6 nm in the p-a-Si/n-a-Si layers.[21,22,24] For simplicity, interface/surface recombination is not considered, which does not affect the main conclusions of this work. The above optical and electrical simulations are performed using a commercial software package (FDTD Solutions v8 and DEVICE v3, Lumerical 2013).

After optical and electrical simulations, the performance parameters of the SNW and CSNW array cell are calculated. To ensure direct comparability with the traditional definition of cell parameters of large-size devices, the short-circuit current density (J_{sc}) of the SNW and CSNW array cell is defined by

$$J_{sc} = \frac{I_{sc}}{P^2}, \tag{1}$$

where I_{sc} is the simulated short-circuit current of a unit cell and P is the array period (unit length). It can be readily seen that under such definition, the J_{sc} of an a-Si SNW/CSNW array cell has an upper limit of 21.84 mA/cm^2, the same as any other macro-scale a-Si solar cells. Similarly, the energy conversion efficiency η of the SNW and CSNW array cell is defined by

$$\eta = \frac{I_m \times V_m}{P^2 \times 100\,\text{mW/cm}^2}, \tag{2}$$

where I_m and V_m are the current and voltage of a unit cell at maximum power point, P is the array period, and 100 mW/cm^2 is the energy flux of AM1.5G illumination. Under such definition, the energy conversion efficiency η of the SNW and CSNW array cell has the classical meaning: the ratio between the output power and the total incident energy flux over the entire cell surface.

In calculating the photonic band structure of the exemplary SNW array, the a-Si material is set to have a constant permittivity of $\varepsilon = 11.9$ and the extinction coefficient is set as zero. The photonic bands are calculated by the plane wave expansion method using a commercial software package (RSoft).

III. RESULTS AND DISCUSSION

Fig. 1(a) shows the schematic of a single SNW solar cell. To compare with the planar efficiency limit, we have adopted the same p-i-n structure of the traditional a-Si thin film solar cell, where the layer thicknesses are fixed at p = 20 nm/i = 460 nm/n = 20 nm, respectively.[21] It is important to note that the choice of a-Si cell is merely due to its matureness in parameterization and modeling, while the discussion can apply to a large range of other cell materials and result in higher efficiencies.[1,2,4,5] Also, crucial limiting factors for a realistic solar cell, such as non-radiative recombination, have been taken into account to ensure direct comparability with the experimental results. In our previous work, we have found that the concentration factor of this structure is maximized when the nanowire radius is ~50 nm, so that it supports the $HE_{11\delta}$ resonance of the main absorption wavelength.[3] In the following, this choice of nanowire radius is retained to take full advantage of the light concentration effect and to promote the V_{oc} furthest above the S-Q limit. For the same reason, a metal back reflector is always applied beneath the nanowire, which, together with the 80 nm-thick TCO top layer, also serves as the electrical contacts of the cell. The absorption efficiency (Q_{abs}) of this structure, defined as the ratio between its optical and geometrical cross-sections, is shown in Fig. 1(b). Absorption in the nanowire is remarkably enhanced when the $HE_{11\delta}$ and $HE_{12\delta}$ modes are excited by $\lambda = 626$ nm and $\lambda = 365$ nm, respectively, whereas it drops significantly for wavelengths near the band gap of a-Si ($\lambda = 720$ nm) due to the weak absorption of the material in this region. Integrating the Q_{abs} with AM1.5 solar spectrum gives an overall 21-fold built-in concentration, leading to a high V_{oc} of 1006 mV, an extremely high J_{sc} of 432.7 mA/cm^2, a high IQE of 96.5%, and a high conversion efficiency η of 17.67% (as compared to the planar limits of 882 mV, 18.84 mA/cm^2, 86.8%, and 13.32%, respectively).

The knowledge of the optical and electrical behaviors of a single SNW solar cell provides a useful basis in analyzing the more complicated characteristics of their arrays. Specifically, the conversion efficiency of a SNW array solar cell is maximized when (1) the reflectance from the solar cell is minimized, (2) the V_{oc} promotion in each unit cell is preserved, and (3) the carrier extraction advantage (higher IQE than planar) is retained. The first condition requires a high absorption capability of the SNW array across the broad AM1.5 spectrum, in contrast to the mode-dependent characteristic absorption of a single SNW.[1,3,17] The second condition requires a sufficiently large spacing (period) between adjacent SNWs, so that their optical cross-sections do not substantially overlap and still function as effective light-concentrators. The last condition requires that most of the photocarriers are generated within the i-layer of the SNW array cell. With these criteria in mind, we first investigate the performance of the SNW array cell depicted in Fig. 1(c). The array cell is characterized by its period (P), and its optical property is described by the wavelength-dependent absorption (Abs), where $Abs = 1 - R$ and R is the wavelength-dependent reflectance from the cell. In Fig. 1(d), the Abs of the SNW array cell is shown in color against increasing P. There are several key features to be noted in this contour. First, strong absorption of the array is observed for resonant wavelengths of the $HE_{11\delta}$ and $HE_{12\delta}$ modes, indicated by Abs values close to unity. This is especially true for the $HE_{11\delta}$ mode, where an array as sparse as 700 nm in period can still absorb almost all the incident light with $\lambda = 626$ nm. Second, a relatively high absorption region is found for the non-resonant wavelengths, where $P < \lambda$ is satisfied. Third, the array shows very poor absorption of wavelengths near the a-Si band gap, where even the densest array of $P = 250$ nm only captures less than 1/3 of the incident light.

Apparently, these optical features of the SNW array cell come from both the property of the unit cell and that of their collective group.[4,10,25] Since the former has been well studied previously, we now focus on the latter issue. A square array of SNWs can be considered as a grating with discrete translational symmetries in both two in-plane directions ($\vec{x}$ and $\vec{y}$).[4,11,25,26] And Bloch's theorem dictates that the in-plane wave vector $\vec{k}_{||}$ is conserved up to the addition of reciprocal lattice vectors, which is commonly known as the *Bragg-diffraction* condition.[11,26] Explicitly, for a square array

$$\vec{k}'_{||} = \vec{k}_{||} + m_1 \frac{2\pi}{p}\vec{x} + m_2 \frac{2\pi}{p}\vec{y}, \tag{3}$$

where $\vec{k}'_{||}$ and $\vec{k}_{||}$ are the in-plane wave vectors of the diffracted and incident light, m_1 and m_2 are any combination of integers, and p is the array period. Such ability of the array to provide in-plane momentum for incident light has been exploited in many light-trapping schemes, where it enables phase-matched coupling of light into the guided modes (if it is used in conjunction with a thin layer of substrate) or the diffraction modes (if it is used in conjunction with an infinitely thick substrate) of the absorbing material.[4,10,11] However, in our case, the SNW array is itself the absorber and its interaction with light must be understood via its photonic band structure, which is plotted in Fig. 1(e) for $P = 300$ nm.[26,27] The purple lines show the first 40 photonic bands across the irreducible Brillouin zone between the labeled high-symmetry points, while the blue shaded area shows the continuum of radiation modes, or normally referred to as the light cone. Like in any photonic crystal slab, the modes below the light cone are truly guided modes with infinite lifetime.[26,27] If a specific wavelength can acquire a suitable in-plane momentum, it can be coupled into these guided modes for significant absorption enhancement.[26–28] However, the SNW array alone cannot provide this phase-matching, as can be readily seen from Equation (3) that any diffracted wave vector $\vec{k}'_{||}$ for normal incident light ($\vec{k}_{||} = 0$) still falls on the Γ point in the reduced zone scheme. At the Γ point, all photonic states supported by the array reside in the light cone. These modes can couple to radiation modes in air and thus possess only a finite lifetime, which are often called guided resonances.[26,27,29,30] The above information of the photonic band structure offers a straightforward explanation to the optical properties of the array shown in Fig. 1(d). When normal incident light reaches the air/array interface, which is essentially a grating, it is either diffractively reflected or coupled to the supported modes of the array.[11,16,17,26] The reflection loss on this interface (termed "in-coupling loss" by Anttu and Xu[17]) determines how much light can enter the SNW array, and its value strongly depends on the number (order) of the diffractive reflections.[11,16,17,26] When $P < \lambda$, all but the 0th order reflections vanish, since Equation (3) gives an imaginary normal-to-plane wave vector $\vec{k}'_{\perp}$ ($(\vec{k}'_{\perp})^2 = \left(\frac{2\pi}{\lambda}\right)^2 - (\vec{k}'_{||})^2$) for these modes (evanescent waves). By contrast, the array supports a large number of guided resonant modes for these wavelengths (note that $P < \lambda$ equals to the normalized frequency $\frac{\omega p}{2\pi c} < 1$ in Fig. 1(e)).[26,27] Consequently, light is more effectively coupled into the array than reflected due to the contrast in the density of optical states, resulting in the broadband relatively high absorption region denoted by $P < \lambda$. Such phenomenon is quite similar to the case of an array/substrate system, where the high-index substrate supports more diffraction modes than air and causes a dip in reflectance for $P = \lambda$ (Rayleigh anomaly).[11,26] On the other hand, not all the incident light that passes through the air/array interface gets absorbed. The finite lifetime of the guided resonant states suggests that the in-coupled light will eventually escape from the array if it is too weakly absorbed by the material.[26,27,29,30] And this has been clearly evidenced by the poor absorption performance near the a-Si band gap in Fig. 1(d).

Now based on the *Abs* profile, we can conclude that the preliminary SNW array structure is not yet optimized for large scale photovoltaics due to the lack of uniform absorption capability across the solar spectrum. This is shown explicitly in Fig. 1(f), where the AM1.5-integrated *Abs*, the open-circuit voltage V_{oc}, and the cell efficiency η are plotted as black, red, and blue solid lines, respectively, for the SNW array cell. The *Abs* drops rapidly with increasing P, showing a reflection loss of ~10% at $P = 230$ nm and ~20% at $P = 320$ nm, whereas the corresponding V_{oc} increments are only 83 mV and 102 mV, respectively. Clearly, the reflection loss compensates the benefit in V_{oc} for larger values of P, leaving the maximum of η to be found at $P = 175$ nm with $\eta = 15.92\%$, $Abs = 0.96$, $V_{oc} = 944$ mV, and IQE = 95.1%, respectively. Although this efficiency maximum is ~20% higher than the planar limit of $\eta = 13.32\%$, we can still see that this enhancement primarily comes from the improved IQE (which will be discussed later), and that the V_{oc} promotion is only half of that in a single SNW due to the denseness of the array, showing plenty of room for improvement.

As has been discussed above, to fully exploit the built-in concentration of SNWs, we need to choose a sparse array with a large P, which in turn requires that the light-trapping mechanisms of the individual SNWs and the array be more delicately coordinated, so that each section of the spectrum is covered by a certain mechanism. These two sources of light-trapping represent two distinct solutions. For the light-trapping of the array, we can see from its band structure in Fig. 1(e) that if we introduce additional scatterers (e.g., a grating back reflector with a different P), the normal incident light may acquire a matching in-plane momentum and couple to the guided modes of the array.[11,26] This should notably improve the absorption across the spectrum, especially near the material band gap, but we will not discuss this approach here due to the additional complexity in experimental realization. The other way is to adjust the cavity-like light-trapping of the single SNWs, i.e., the $HE_{11\delta}$ and $HE_{12\delta}$ modes. As can be seen in Fig. 1(d), due to the array light-trapping boundary of $P < \lambda$, for large P ($P > 450$ nm), there is a lack of absorption for the medium wavelengths ($\lambda = 450$ nm–500 nm) apart from the poor absorption near the band gap, whereas the HE modes provide either insignificant ($\lambda = 365$ nm, low photon flux) or redundant ($\lambda = 626$ nm, covered by array light-trapping) absorption enhancement for such value of P (~450 nm). This inspires us to move the HE resonant peaks to longer wavelengths, complementing the array light-trapping. A similar conclusion has been drawn previously by Anttu *et al*. that a SNW array shows maximum overall absorption when one of the resonant absorption peaks of a single wire is placed near the material band gap.[16,17] However, in these works, the resonant peaks are controlled through the nanowire radius,[5,12,13,15–19] which is infeasible in our case since the effectiveness of the built-in concentration diminishes rapidly with increasing radius (according to our previous work, the concentration factor drops from 21 to ~16 when the $HE_{11\delta}$ mode is placed near the band gap, and further to ~4.5 when the $HE_{12\delta}$ mode is placed near the band gap).[3] Thus, we need to choose another radius-unconstrained method in tuning the resonances of the single SNWs. Considering their DRA nature, we refer to the alternative solution in DRA applications for resonance tuning, i.e., the embedded DRA (EDRA) technique.[31–33] The resonant frequencies of a DRA can be modified by placing it into an embedded structure without having to change its geometrical parameters. Explicitly, for a cylindrical DRA, previous works have shown a red shift in its resonant wavelengths when embedded into a larger coaxial cylinder with a lower refractive index.[31–33] This suggests the conformal coating of the SNWs with a dielectric shell, which is the adopted method in the following discussion.

Fig. 2(a) shows the schematic of the CSNW structure. We have chosen SiN_x as the coating material in the simulations, but the conclusions should readily extend to other dielectric materials with similar refractive indexes, e.g., SiO_2. In Fig. 2(b), the influence of the coating thickness C on the Q_{abs} of a single CSNW is drawn in color. The peak positions of the first two resonances are plotted in dashed black lines and can be traced back to the $HE_{11\delta}$ and $HE_{12\delta}$ modes of the uncoated SNWs, respectively.[3] It can be seen that the resonant wavelength and the resonant magnitude (indicated by Q_{abs}) both increase with increasing coating thickness C, consistent with the previous findings.[31–33] Accordingly, we can choose a suitable value of C to move these resonances to the required parts of the absorption spectrum, as is shown in Fig. 2(c). By choosing $C = 65$ nm, the $HE_{12\delta}$ mode is moved to the medium wavelength ($\lambda = 484$ nm), enhancing the local Q_{abs} by ~3 fold, and the $HE_{11\delta}$ mode is moved into the material band gap, enhancing the near-band-gap Q_{abs} by more than 3 fold. Thus, the new CSNW structure can satisfy our previous requirements for the light-trapping of a unit cell.

Next we evaluate the performance of the CSNW array, which is depicted in Fig. 3(a). As before, the array is characterized by the period P, and its optical property is reflected in the *Abs* contour in Fig. 3(b). Similar to that of the SNW array in Fig. 1(d), the strong absorption region of the CSNW array is determined by both the HE-mode-dependent resonant absorption of the individual CSNWs and the array light-trapping boundary of $P < \lambda$. However, in this case, the relocated HE modes provide critical absorption enhancement for the array. The strong light-trapping of the individual CSNWs at resonance allows for almost complete absorption of the medium and near-band-gap wavelengths up to a period of 600 nm, at which point the array light-trapping has been demonstrated to be ineffective due to either the existence of higher order diffractive reflections or the leaky nature of its guided resonances.[11,26,27,29,30] Consequently, the CSNW

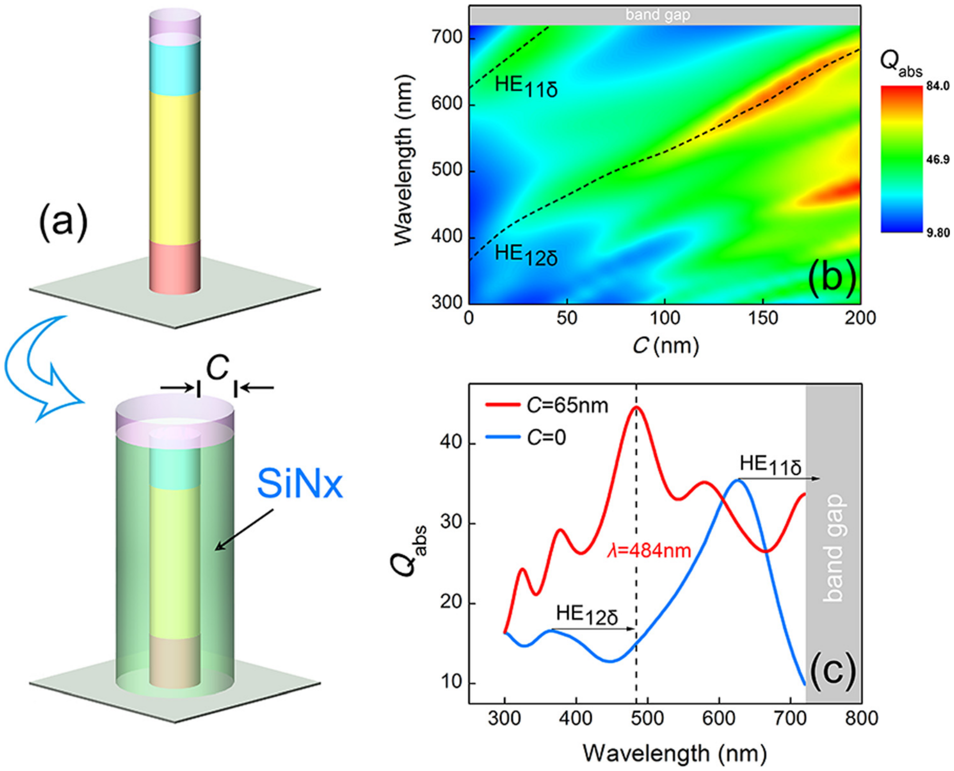

FIG. 2. (a) Schematic 3D drawing of the single CSNW solar cell. The CSNW cell is formed by embedding a SNW cell into a coaxial dielectric shell with a thickness of C. (b) Shifting of the DRA modes of the CSNW cell as a function of coating thickness. The first two resonances are labeled by dashed black lines and can be traced back to the $HE_{11\delta}$ and $HE_{12\delta}$ modes of the single SNW cell, respectively. (c) Absorption efficiency Q_{abs} of the single SNW cell and single CSNW cell ($C = 65$ nm). The $HE_{11\delta}$ and $HE_{12\delta}$ modes can be moved to the desired parts of the absorption spectrum (near band gap and medium wavelength) by choosing $C = 65$ nm.

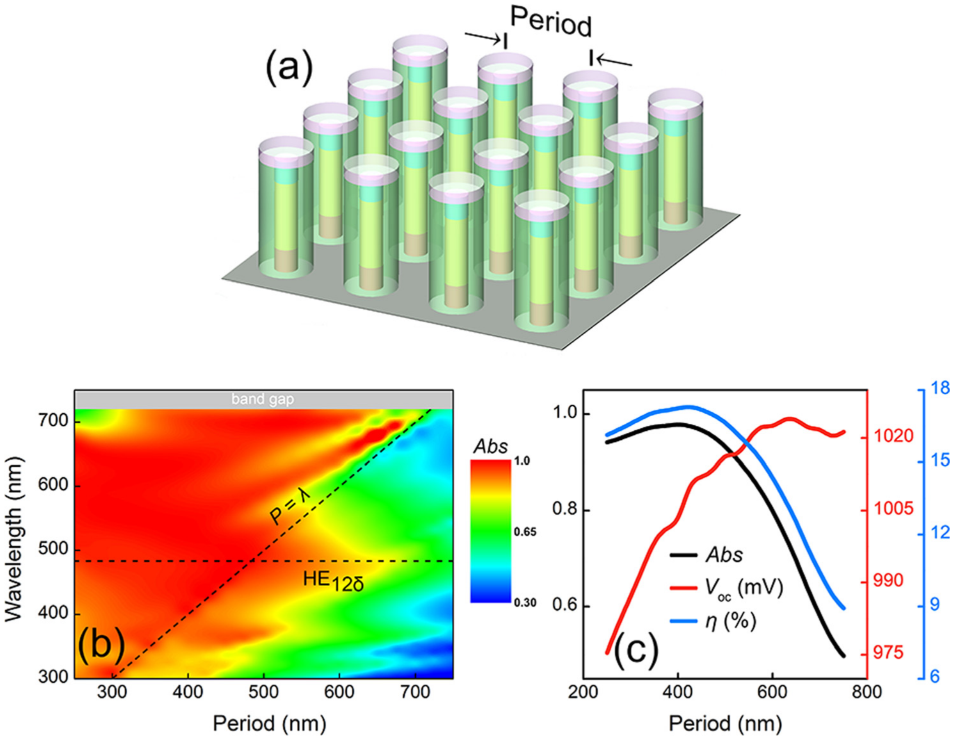

FIG. 3. (a) Schematic 3D drawing of the CSNW array solar cell. (b) Wavelength-dependent absorption *Abs* of the CSNW array cell as a function of array period P. The $HE_{11\delta}$ resonant wavelength is moved beyond the a-Si band gap and is not shown in the figure. (c) Simulated AM1.5-integrated absorption *Abs*, open-circuit voltage V_{oc}, and cell efficiency η of the CSNW array solar cell as functions of the array period P.

array can sustain a broadband high absorption capability for P values as large as 500 nm (which is about the extent of the optical cross-section of a single SNW[3]), thus enabling full utilization of the built-in concentration effect. In Fig. 3(c), the resulted AM1.5-integrated *Abs*, the open-circuit voltage V_{oc}, and the cell efficiency η are plotted for the CSNW array cell. Due to the complementary light-trapping effects across the absorption spectrum, the CSNW array cell shows reflectance values less than 6% for P ranging from 250 nm to 500 nm, with a minimum of 2.2% at $P = 400$ nm. The efficiency maximum is found at $P = 425$ nm, with $\eta = 17.29\%$, $Abs = 0.975$, $V_{oc} = 1009$ mV, and IQE = 96.2%, respectively. This equals to a 30% relative increase over a planar device with the exact same material and an absorption capability of unity, namely, the practical efficiency limit of planar structure. Further comparing the CSNW array cell with the single SNW cell, we can see that the promotion in V_{oc} is not only preserved but slightly enhanced by the excitation of the guided resonances of the array, and that the high IQE feature is retained (as will be shown later). Thus, we have shown from the theoretical point of view the possibility to realize a macro-scale solar cell that performs far beyond the planar V_{oc} and IQE limit.

Here, it is worth pointing out that certain properties of the CSNWs may notably facilitate their experimental realization. First, the coating can in principle be formed by more than one type of lower-index materials, e.g., a TCO/SiO_2 shell as is used by Wallentin *et al.* in their InP cell.[2] The shifting of the DRA modes in this case needs to be further determined, but it provides much convenience for the realization of the cell structure. Second, in tuning the HE resonances of the single CSNWs, we have chosen $C = 65$ nm, so that the $HE_{11\delta}$ and $HE_{12\delta}$ modes are precisely moved to the band gap and the medium wavelength, respectively. However, this choice may not be unique. As can be seen in Fig. 2(b), more resonances show up when further increasing C, and for $C \sim 180$ nm the Q_{abs}s at the medium wavelength and near the band gap are comparable to or even higher than those of $C = 65$ nm. For such thick coatings, the CSNWs touch each other in the array and should not be analyzed separately,[14,26] nevertheless simulations show that the reflectance values in such cases are around 10%. This means that there may be a range of feasible coating thicknesses, which also loosens the constraint on experimental designs. Finally, we have fixed the SNW radius at 50 nm in this work to maximize the built-in concentration and thus V_{oc}. Nevertheless, further fine tuning of the SNW radius may lead to slight increase of array performance, since the potential lowering of V_{oc} may be compensated by further increase of array absorption. For clarity of the main mechanism, we have not included this part in the present work.

As the first step in extending the single SNW solar cell concept to macro-scale applications, we have until now primarily focused on engineering the optical absorption of the cell. This is due to the fact that the requirement of preserving the built-in concentration of the unit cells while retaining an excellent broadband absorption has set the most critical limits on the design of the cell, and that the reflection loss is by far the strictest limiting factor in the preliminary SNW array structure (as is shown in Fig. 1(f)). During optimizing the optical absorption, we have shown that the high IQE feature of the single SNW cell can be inherited by the SNW/CSNW arrays and contributes notably to the promotion of the cell efficiency beyond the planar limit. Next we will discuss this issue and reveal some crucial factors. In Fig. 4(a), we have displayed the cross-sectional views of the optical absorption profiles of the planar cell, the single SNW cell, the single

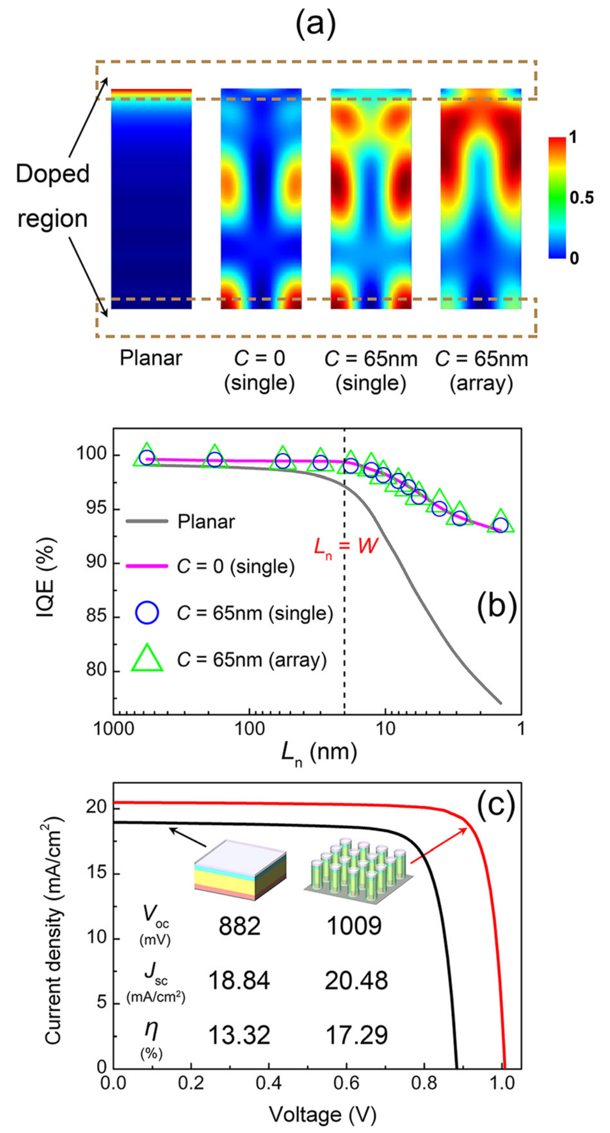

FIG. 4. (a) Cross-sectional views of the optical absorption profiles of the planar cell, the single SNW cell, the single CSNW cell ($C = 65$ nm), and the CSNW array cell ($C = 65$ nm) under AM1.5 illumination. The normalized electrical field intensity is displayed as color and the dashed frames show the region of the doped layers. (b) IQE of the planar cell, the single SNW cell, the single CSNW cell ($C = 65$ nm), and the CSNW array cell ($C = 65$ nm) under AM1.5 illumination as functions of the minority carrier diffusion lengths in the doped layers. L_n and L_p are kept proportional and only L_n is shown as the abscissa. The doped layer thickness W is denoted by a vertical dashed line. (c) Simulated I-V curves and the cell parameters of the planar cell and the CSNW array cell under AM1.5 illumination. The planar cell is operating under the total-absorption condition (zero reflection, see Section II).

CSNW cell ($C = 65$ nm), and the CSNW array cell ($C = 65$ nm), respectively, under AM1.5 illumination. The colors show the electrical field intensity, each normalized separately, and the dashed frames show the region of the doped layers. As we have shown in our previous work,[3] the absorption region of the single SNW cell (second from left) is determined by the excited mode profile, i.e., the $HE_{11\delta}$ mode for a radius of 50 nm. This is not only because of the dominance in intensity of the resonant wavelength in the AM1.5 spectrum but more importantly because the single SNW has the largest optical cross-section for the $HE_{11\delta}$ resonant wavelength. Consequently, light absorption in the single SNW cell is effectively confined within the intrinsic middle layer of the cell, leading to a significant promotion in IQE compared to the planar structure (leftmost). Similar analysis for the single CSNW cell predicts that its absorption region should be in between the mode profiles of the $HE_{11\delta}$ and $HE_{12\delta}$ modes, since its optical cross-section is the largest around these two resonances. This is partly embodied in Fig. 4(a) (second from right), where its optical pattern is slightly different from that of the single SNW cell and is more evenly distributed within the intrinsic layer of the cell. Note that a second maximum is not seen in the radial direction (as it should be for the $HE_{12\delta}$ mode), which is probably because of the overlap of different modes or that the absorption coefficient of the resonant wavelength is too large for light energy to reach the nanowire center.[15] When the CSNWs are put into an array (rightmost), the optical patterns further shift away from that of a single mode. This is because the wavelength-selectivity of a single CSNW no longer affects the absorption pattern of the array. In this case, the array has uniformly high absorption in the range of 300 nm–720 nm, without extra optical cross-section for the resonant wavelengths, thus showing a less characterized optical pattern. Nevertheless, for both the single CSNW cell and the CSNW array cell, the absorption region is well confined to the intrinsic middle layer, allowing for the preservation of the IQE advantage of the single SNW cell.

In Fig. 4(b), we have shown this feature by varying the minority carrier diffusion lengths within the doped layers. L_n (electrons) and L_p (holes) are varied from their default values of 6.3 nm/5.8 nm to a range of 600 nm–1 nm by simultaneously changing the doping concentrations in the p-a-Si/n-a-Si layers (their values are kept proportional in all the cases). The carrier extraction advantage of the single SNW cell is embodied by its much higher IQE than that of the planar one, especially for diffusion lengths smaller than the doped layer thickness W. Such high tolerance for doping-induced recombination comes from the congruity between the cell's electrical structure and its absorption profile, which is an important advantage for the single SNW cell to perform beyond the planar efficiency limit.[3,34,35] Here, we can see in Fig. 4(b) that the single CSNW cell and the CSNW array cell possess the same high IQE feature, showing IQE values of 96.2% and 96.1% under the default diffusion lengths, as compared to 86.8% of the planar cell and 96.5% of the single SNW cell. This is a straightforward result of the optical patterns of the cells shown in Fig. 4(a), proving that the enhanced carrier extraction of the single SNW cell can be retained in the macro-scale CSNW array solar cell.

At last, we compare the simulated performance of the planar cell limit (total-absorption condition) and the CSNW array cell under AM1.5 illumination (see Section II for definition of cell parameters). Their I-V curves are shown in Fig. 4(c), together with their cell parameters. The V_{oc} of the CSNW array cell is 127 mV higher than the planar cell limit under the same experimental parameters due to the well preserved built-in concentration of each unit cell. On the other hand, even with ~2.5% reflection, the J_{sc} (calculated from the whole cell area) of the CSNW array cell is 1.64 mA/cm^2

higher than the total-absorbing planar counterpart, which is due to the more efficient carrier extraction. As a result, the conversion efficiency of the CSNW array cell is as high as 17.29%, showing a 30% relative increase over the planar limit of 13.32% (which is close to the initial efficiency of the record experimental a-Si solar cell[20]). Such significant improvement in energy conversion is beyond the scope of conventional efficiency-improving techniques (e.g., antireflection or passivation) and has been achieved by constructing a macro-scale device from nano-scale units each of which can perform beyond the planar efficiency limits.[1,3] As to the experimental fabrication, such CSNW array can be formed by molecular beam epitaxy,[5] dry etching,[18] metal-assisted chemical etching,[36] and vapor-liquid-solid growth,[37,38] followed by film deposition using plasma-enhanced chemical vapor deposition (PECVD) or evaporation. Compared to other novel designs of nanowire solar cells that predict even higher efficiencies by effective spectrum splitting,[39,40] the CSNW array design offers a simpler and more applicable way of improving solar cell efficiency. Here, it is worth pointing out that the predicted increment in cell efficiency over the planar design is built on a premise of an effective surface passivation, since the CSNW array has an enlarged surface area compared to a planar cell. Fortunately, latest development on nanostructured solar cells have proven that with tailored passivation coatings, the surface recombination velocity can be lowered to an extent where it does not significantly affect the device performance and the cell efficiency shows an actual improvement compared to the traditional designs.[41–43] Such passivation coatings include atomic-layer-deposited Al_2O_3 (Refs. 41 and 42) or PECVD SiO_x/SiN_x.[43] Although the structure is identical, we have excluded the discussion of surface recombination in the present work to highlight the main optical designs. It would be an interesting and useful future work to quantitatively determine the required surface recombination velocity for the above results to hold. Finally, considering its high efficiency, experimental feasibility, and extreme material-saving (more than 20-fold in this work), the conceptual CSNW array solar cell has shown remarkable potential for next-generation photovoltaics.

IV. CONCLUSIONS

We have theoretically examined the possibility of expanding the single SNW solar cell concept into a macro-scale device that performs furthest beyond the planar efficiency limits. These limits include the S-Q V_{oc} limit imposed by the constant solid angle of the solar radiation incident on planar solar cells, and the carrier collection limit imposed by the junction and absorption profiles of traditional cell structures. The key factor is the artificial relocation of the HE resonant modes of the individual SNWs to the regions of the absorption spectrum where the photonic light-trapping of the array is ineffective. With such complementary light-trapping design, the array can simultaneously sustain a broadband high absorption capability and a sparse geometry that facilitate the effectiveness of the built-in concentration, leading to maximized conversion efficiency. Moreover, we have shown that the traditional radius-dependent method for tuning the resonances of single SNWs should be replaced by the EDRA technique, as a premise for preserving the built-in concentration in each unit cell. On the other hand, the carrier extraction advantage of the single SNW cell can be inherited by the CSNW array cell due to their similarity in optical profile. As a result, the optimized CSNW solar cell shows a 30% relative increase in conversion efficiency over the total-absorbing planar counterpart. These findings can serve as a theoretical guidance to fabricate high-efficiency solar cells based on SNWs.

ACKNOWLEDGMENTS

This work was supported by National Major Basic Research Projects (2012CB934302) and Natural Science Foundation of China (Nos. 11174202, 61234005, and 11474201).

[1] P. Krogstrup, H. I. Jorgensen, M. Heiss, O. Demichel, J. V. Holm, M. Aagesen, J. Nygard, and A. F. I. Morral, Nat. Photonics **7**, 306–310 (2013).
[2] J. Wallentin, N. Anttu, D. Asoli, M. Huffman, I. Aberg, M. H. Magnusson, G. Siefer, P. Fuss-Kailuweit, F. Dimroth, B. Witzigmann, H. Q. Xu, L. Samuelson, K. Deppert, and M. T. Borgstrom, Science **339**, 1057–1060 (2013).
[3] Y. Zeng, Q. Ye, and W. Shen, Sci. Rep. **4**, 4915 (2014).
[4] M. L. Brongersma, Y. Cui, and S. H. Fan, Nat. Mater. **13**, 451–460 (2014).
[5] M. Heiss, E. Russo-Averchi, A. Dalmau-Mallorqui, G. Tutuncuoglu, F. Matteini, D. Ruffer, S. Conesa-Boj, O. Demichel, E. Alarcon-Llado, and A. Fontcuberta i Morral, Nanotechnology **25**, 014015 (2014).
[6] U. Rau, U. W. Paetzold, and T. Kirchartz, Phys. Rev. B **90**, 035211 (2014).
[7] W. Shockley and H. J. Queisser, J. Appl. Phys. **32**, 510–519 (1961).
[8] W. Ruppel and P. Wurfel, IEEE Trans. Electron Dev. **27**, 877–882 (1980).
[9] S. F. Leung, Q. P. Zhang, F. Xiu, D. L. Yu, J. C. Ho, D. D. Li, and Z. Y. Fan, J. Phys. Chem. Lett. **5**, 1479–1495 (2014).
[10] F. Proise, F. Pardo, A. L. Joudrier, C. Njel, J. Alvarez, A. Delamarre, A. M. Goncalves, A. Lemaitre, N. Bardou, C. Dupuis, A. Etcheberry, J. F. Guillemoles, and J. L. Pelouard, Proc. SPIE **8981**, 89811G (2014).
[11] S. Mokkapati and K. R. Catchpole, J. Appl. Phys. **112**, 101101 (2012).
[12] N. Anttu, A. Abrand, D. Asoli, M. Heurlin, I. Åberg, L. Samuelson, and M. Borgström, Nano Res. **7**, 816–823 (2014).
[13] N. Anttu, S. Lehmann, K. Storm, K. A. Dick, L. Samuelson, P. M. Wu, and M. E. Pistol, Nano Lett. **14**, 5650–5655 (2014).
[14] B. C. P. Sturmberg, K. B. Dossou, L. C. Botten, A. A. Asatryan, C. G. Poulton, R. C. McPhedran, and C. M. de Sterke, ACS Photonics **1**, 683–689 (2014).
[15] B. M. Wang and P. W. Leu, Opt. Lett. **37**, 3756–3758 (2012).
[16] N. Anttu, Opt. Lett. **38**, 730–732 (2013).
[17] N. Anttu and H. Q. Xu, Opt. Express **21**, A558–A575 (2013).
[18] N. Dhindsa, A. Chia, J. Boulanger, I. Khodadad, R. LaPierre, and S. S. Saini, Nanotechnology **25**, 305303 (2014).
[19] P. M. Wu, N. Anttu, H. Q. Xu, L. Samuelson, and M. E. Pistol, Nano Lett. **12**, 1990–1995 (2012).
[20] A. Nowzari, M. Heurlin, V. Jain, K. Storm, A. Hosseinnia, N. Anttu, M. T. Borgström, H. Pettersson, and L. Samuelson, Nano Lett. **15**, 1809–1814 (2015).
[21] S. Benagli, D. Borrello, E. Vallat-Sauvain, J. Meier, U. Kroll, J. Hoetzel, J. Bailat, J. Steinhauser, M. Marmelo, G. Monteduro, and L. Castens, in *24th European Photovoltaic Solar Energy Conference*, Hamburg (2009), pp. 21–25.
[22] C. M. Hsu, C. Battaglia, C. Pahud, Z. C. Ruan, F. J. Haug, S. H. Fan, C. Ballif, and Y. Cui, Adv. Energy Mater. **2**, 628–633 (2012).
[23] E. D. Palik, *Handbook of Optical Constants of Solids* (Academic Press, 1998), Vol. 3, p. 451.
[24] A. Datta, M. Rahmouni, M. Nath, R. Boubekri, P. R. I. Cabarrocas, and P. Chatterjee, Sol. Energy Mater. Sol. Cells **94**, 1457–1462 (2010).

[25] A. P. Vasudev, J. A. Schuller, and M. L. Brongersma, Opt. Express **20**, A385–A394 (2012).

[26] J. D. Joannopoulos, S. G. Johnson, J. N. Winn, and R. D. Meade, *Photonic Crystals: Molding the Flow of Light*, 2nd ed. (Princeton University Press, 2008), p. 137.

[27] S. H. Fan and J. D. Joannopoulos, Phys. Rev. B **65**, 235112 (2002).

[28] Z. F. Yu, A. Raman, and S. H. Fan, Proc. Natl. Acad. Sci. U. S. A. **107**, 17491–17496 (2010).

[29] P. Paddon and J. F. Young, Phys. Rev. B **61**, 2090–2101 (2000).

[30] M. Kanskar, P. Paddon, V. Pacradouni, R. Morin, A. Busch, J. F. Young, S. R. Johnson, J. MacKenzie, and T. Tiedje, Appl. Phys. Lett. **70**, 1438–1440 (1997).

[31] A. Petosa, *Dielectric Resonator Antenna Handbook* (Artech House, 2007), p. 134.

[32] A. G. Walsh, C. S. De Young, and S. A. Long, IEEE Antennas Wireless Propag. **5**, 130–133 (2006).

[33] S. M. Shum and K. M. Luk, IEE Proc. Microwave Antennas Propag. **142**, 189 (1995).

[34] D. E. Carlson and C. R. Wronski, Appl. Phys. Lett. **28**, 671–3 (1976).

[35] Z. C. Holman, A. Descoeudres, L. Barraud, F. Z. Fernandez, J. P. Seif, S. De Wolf, and C. Ballif, IEEE J. Photovoltaic **2**, 7–15 (2012).

[36] F. Priolo, T. Gregorkiewicz, M. Galli, and T. F. Krauss, Nat. Nanotechnol. **9**, 19–32 (2014).

[37] N. Jiang, J. Wong-Leung, H. J. Joyce, Q. Gao, H. H. Tan, and C. Jagadish, Nano Lett. **14**, 5865–5872 (2014).

[38] S. Misra, L. W. Yu, W. H. Chen, M. Foldyna, and P. R. I. Cabarrocas, J. Phys. D: Appl. Phys. **47**, 393001 (2014).

[39] A. Dorodnyy, E. Alarcon-Lladó, V. Shklover, C. Hafner, A. Fontcuberta i Morral, and J. Leuthold, ACS Photonics **2**, 1284–1288 (2015).

[40] S. A. Mann and E. C. Garnett, ACS Photonics **2**, 816–821 (2015).

[41] H. Savin, P. Repo, G. V. Gastrow, P. Ortega, E. Calle, M. Garín, and R. Alcubilla, Nat. Nanotechnol. **10**, 624–628 (2015).

[42] Z. Huang, S. Zhong, X. Hua, X. Lin, X. Kong, N. Dai, and W. Shen, Prog. Photovoltaic: Res. Appl. **23**, 964–972 (2015).

[43] Z. Huang, X. Song, S. Zhong, H. Xu, W. Luo, X. Zhu, and W. Shen, Adv. Funct. Mater. **26**, 1892–1898 (2016).